Anomalous Interface and Surface Strontium Segregation in (La1−y Sr y) 2CoO4±δ/La1−x Sr x CoO3− δ Heterostructured Thin Films

ARTICLE *in* JOURNAL OF PHYSICAL CHEMISTRY LETTERS · MARCH 2014

Impact Factor: 7.46 · DOI: 10.1021/jz500293d

9 AUTHORS, INCLUDING:

Gadre Milind
University of Wisconsin–Madison
10 PUBLICATIONS **98** CITATIONS
SEE PROFILE

Wesley T Hong
Massachusetts Institute of Technology
23 PUBLICATIONS **267** CITATIONS
SEE PROFILE

Hua Zhou
Argonne National Laboratory
69 PUBLICATIONS **689** CITATIONS
SEE PROFILE

Michael D. Biegalski
Oak Ridge National Laboratory
129 PUBLICATIONS **2,507** CITATIONS
SEE PROFILE

THE JOURNAL OF PHYSICAL CHEMISTRY Letters

Letter

pubs.acs.org/JPCL

Anomalous Interface and Surface Strontium Segregation in $(La_{1-y}Sr_y)_2CoO_{4\pm\delta}/La_{1-x}Sr_xCoO_{3-\delta}$ Heterostructured Thin Films

Zhenxing Feng,[†,‡] Yizhak Yacoby,[∥] Milind J. Gadre,[▽] Yueh-Lin Lee,[†,‡,▽] Wesley T. Hong,[†,§] Hua Zhou,[⊥] Michael D. Biegalski,[#] Hans M. Christen,[#] Stuart B. Adler,[○] Dane Morgan,*[,▽] and Yang Shao-Horn*[,†,‡,§]

[†]Electrochemical Energy Laboratory, [‡]Department of Mechanical Engineering, and [§]Department of Materials Science and Engineering, Massachusetts Institute of Technology, 77 Massachusetts Avenue, Cambridge, Massachusetts 02139, United States

[∥]Racah Institute of Physics, Hebrew University, Jerusalem 91904, Israel

[⊥]Advanced Photon Source, Argonne National Laboratory, 9700 South Cass Avenue, Argonne, Illinois 60439, United States

[#]Center for Nanophase Materials Science, Oak Ridge National Laboratory, P.O. Box 2008, Oak Ridge, Tennessee 37831, United States

[▽]Department of Materials Science and Engineering, University of Wisconsin—Madison, 1509 University Avenue, Madison, Wisconsin 53706, United States

[○]Department of Chemical Engineering, University of Washington, 105 Benson Hall, Seattle, Washington 98195, United States

Supporting Information

ABSTRACT: Heterostructured oxides have shown unusual electrochemical properties including enhanced catalytic activity, ion transport, and stability. In particular, it has been shown recently that the activity of oxygen electrocatalysis on the Ruddlesden–Popper/perovskite $(La_{1-y}Sr_y)_2CoO_{4\pm\delta}/La_{1-x}Sr_xCoO_{3-\delta}$ heterostructure is remarkably enhanced relative to the Ruddlesden–Popper and perovskite constituents. Here we report the first atomic-scale structure and composition of $(La_{1-y}Sr_y)_2CoO_{4\pm\delta}/La_{1-x}Sr_xCoO_{3-\delta}$ grown on $SrTiO_3$. We observe anomalous strontium segregation from the perovskite to the interface and the Ruddlesden–Popper phase using direct X-ray methods as well as with ab initio calculations. Such Sr segregation occurred during the film growth, and no significant changes were found upon subsequent annealing in O_2. Our findings provide insights into the design of highly active catalysts for oxygen electrocatalysis.

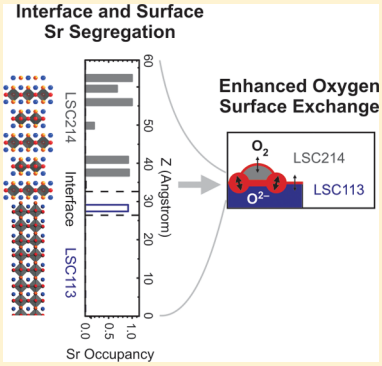

SECTION: Surfaces, Interfaces, Porous Materials, and Catalysis

Interfaces in many heterostructured epitaxial materials exhibit intriguing physical, chemical, and electrochemical properties including enhanced oxygen electrocatalytic activity[1−9] and electronic/ionic conductivity[10−12] compared with bulk materials. As first shown by Sase et al.[13,14] the presence of a Ruddlesden–Popper (RP) $(La_{0.5}Sr_{0.5})_2CoO_{4\pm\delta}$ ($LSCO_{214}$)[15,16] phase on top of the perovskite $La_{0.8}Sr_{0.2}CoO_{3-\delta}$ ($LSCO_{113}$, a mixed electronic and ionic conducting perovskite)[2,10] greatly enhances the activity for the oxygen reduction reaction ($O_2 + 4e^- \leftrightarrow 2O^{2-}$) at the interface between the two phases. Subsequent work has shown that this effect can increase the overall rate of O_2 reduction on LSCO films by three orders of magnitude relative to that on either phase alone.[15,17,18]

A number of studies have been made to understand the high catalytic activity of these LSCO heterostructured catalysts using well-defined thin film systems. Density functional theory (DFT) calculations have shown that there is a large driving force for A-site cationic interdiffusion across the heterostructure interface, stabilizing Sr in $LSCO_{214}$ and La in $LSCO_{113}$ with predicted Sr concentrations ~0.75 near the interface and Sr depletion in $LSCO_{113}$.[19] Such interdiffusion has been postulated to result from coupling of Sr ions to the increased oxygen vacancy content near the surface[20] and is predicted to reduce the oxygen vacancy formation energy.[19] The reduced enthalpy of oxidation at the interface due to the presence of Sr may play a direct role in enhancing the oxygen surface exchange[19] or indirectly via the electronic activation of $LSCO_{214}$.[9] In addition to the Sr segregation within the perovskite-type structures, researchers have previously reported that the surface ORR kinetics can be reduced by the precipitation of Sr-rich secondary phases such as SrO_x.[21,22] These secondary phases are most likely incoherent with the underlying film. These findings highlight the need to determine the Sr redistribution within LSCO heterostructure films, which can provide new insights into developing catalysts with enhanced activity and stability.

However, to date, there have been limited methods for obtaining the atomic-scale compositional and structural

Received: February 11, 2014
Accepted: March 4, 2014

   dx.doi.org/10.1021/jz500293d | J. Phys. Chem. Lett. 2014, 5, 1027−1034

information needed to properly characterize the $LSCO_{214}$/$LSCO_{113}$ interface. XPS[20,23,24] and chemical etching[25] have been used to great effect for studying relative changes in Sr content before and after annealing, with high surface sensitivity. Unfortunately, these techniques lack the structural information for differentiating Sr in the $LSCO_{113}$ and $LSCO_{214}$ phases and the atomic-level of detail necessary to properly identify spatial proximity to the interface.

Recently, we have demonstrated that coherent Bragg rod analysis (COBRA) of $LSCO_{113}$ thin films can provide unprecedented chemical and structural details relevant to high-temperature oxygen electrocatalysis.[26] COBRA is a powerful tool for providing sub-angstrom resolution structural information of systems composed of atoms that are well-registered to a crystal lattice and has been successfully applied in epitaxial thin-film and quantum-dot systems.[27−29] The method utilizes the measured X-ray diffraction intensities along crystal truncation rods to determine the 3D electron density (EDY) of a thin-film structure. Employing the energy-modulated differential COBRA, which provides elemental information through the energy dependence of atomic scattering cross sections, further allows for the determination of atomic concentrations of individual crystallographic sites. Differential COBRA has also been successfully applied to studying thin-film[30] and quantum-dot[31] systems.

We use the COBRA method to study the atomic structure and layer-by-layer strontium distribution in ∼6 nm thick $LSCO_{214}$-$LSCO_{113}$ heterostructure thin films. Significant Sr segregations at the $LSCO_{214}$−$LSCO_{113}$ interface and $LSCO_{214}$ surface have been found. To our knowledge, such information has not been demonstrated by previous work involving conventional techniques such as XPS,[20,22−24] inductively coupled plasma-optical emission spectroscopy (ICP-OES),[32] and time-of-flight secondary ion mass spectroscopy (ToF-SIMS),[25,32] which normally provide the average Sr composition near the surface from perovskite/RP phases and secondary phases on the surface. Supported by ab initio calculations, we demonstrate that anomalous Sr segregation to the interface has a strong thermodynamic driving force and is present in as-deposited films. The COBRA results also reveal polar distortion of the $LSCO_{113}$ unit cell and significant A-site cationic ordering in the $LSCO_{214}$ phase, details that have not been previously considered and may partially contribute to the enhanced catalytic activity of the thin films.

A polished $SrTiO_3$(001) (10 × 10 × 1 mm^3, CrysTec) single-crystal substrate was cleaned, acid-etched, and then O_2 annealed to obtain atomically flat surfaces. An epitaxial thin film of $LSCO_{113}$ on $SrTiO_3$ (STO) was prepared by pulsed laser deposition (PLD) at ∼550 °C under 50 mTorr O_2 for 360 pulses (∼2 nm). Subsequently, 450 pulses of $LSCO_{214}$ (∼2.5 nm) were deposited on $LSCO_{113}$ to form heterostructured $LSCO_{214/113}$. To study the films under the intermediate temperature (400∼600 °C) of the oxygen electrocatalysis condition, the LSCO film was annealed in a vacuum tube furnace (MTI GSL-1700X-KS60) at 550 °C for 1 h in 450 Torr pure O_2 and quenched to room temperature as the "frozen" working status.

In the as-deposited LSCO film, terrace steps from the STO substrate surface were still visible from atomic force microscopy (AFM), indicating conformal growth (Figure S1, Supporting Information). Interestingly, there are two distinct features on the surface; films close to terrace edges are ∼0.8 nm higher than the rest part on the same terraces. This observation suggests that the $LSCO_{214}$ grows by full $LSCO_{214}$ unit cells (rather than by perovskite-like and rock-salt-like building blocks), and nucleation is favored at the top of a terrace step (indicating a large Ehrlich−Schwoebel barrier). This growth mode yields a less uniform surface and therefore poorly defined reflection high-energy electron diffraction (RHEED) oscillations during film growth (Figure S2, Supporting Information). Upon annealing to 550 °C, the surface morphology changed significantly. The AFM image (Figure S1b, Supporting Information) shows the formation of large particles (∼150 nm in diameter and ∼7 nm in height) on top of a base film, which is composed of small particles ∼20 nm in diameter.

Representative experimental and COBRA-calculated diffraction intensities for the as-deposited and annealed LSCO films are in good agreement, where the diffraction intensities along the (11L) Bragg rods are shown as an example in Figure 1.

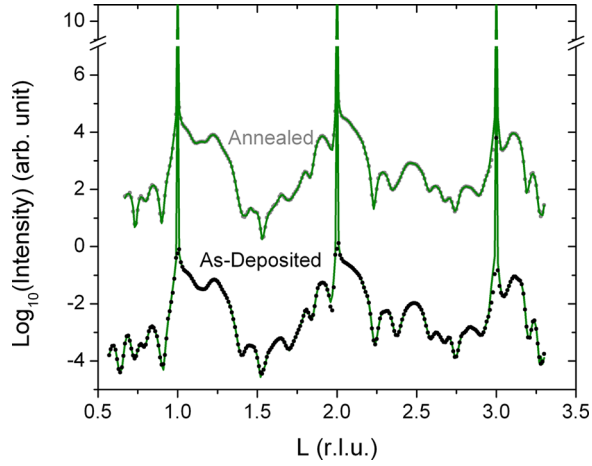

Figure 1. Representative example of the dependence of diffraction intensity on the momentum transfer measured on $(La_{0.5}Sr_{0.5})_2CoO_{4\pm\delta}$ ($LSCO_{214}$)/$La_{0.8}Sr_{0.2}CoO_{3-\delta}$ ($LSCO_{113}$)/$SrTiO_3$(001) for as-deposited and annealed conditions, shown for the (11L) Bragg rod.

Figure 2 shows EDYs along (a) the (0,0,*Z*) line that passes through (La,Sr) atoms in $LSCO_{113}$ and (La,Sr)/Co/O_I in $LSCO_{214}$ and (b) the (0.5,0.5,*Z*) line that passes through Co/Ti/O_I atoms in $LSCO_{113}$ and (La,Sr)/Co/O_I in $LSCO_{214}$. It should be noted that the stacking sequence for atoms along (0,0,*Z*) is A−□−A−□−A for perovskite and A−□−A−O−B−O... for RP, while along (0.5,0.5,*Z*), the sequence is O−B−O−B for perovskite and O−B−O−A−□−A for RP. All atoms and their positions can be clearly identified in the EDY plot, including oxygen, except those at the very surface of the film. The interface of $LSCO_{214}$-on-$LSCO_{113}$ can also be clearly identified, and the atomic structures are consistent with the previous STEM observation.[15] Only one EDY peak at ∼37 Å along the (0,0,*Z*) line (red star in Figure 2a) cannot be assigned unambiguously to either Co or La.

The small EDY fluctuations between peaks shown in Figure 2 provide a measure of the EDY uncertainty,[33,34] which is generally smaller than the oxygen EDY. The EDY along the (0,0,*Z*) line going through the La/Sr atoms (Figure 2a) is larger in the $LSCO_{113}$ film region than in STO, as expected from the larger number of electrons in La relative to Sr. The EDY in the $LSCO_{214}$ region is smaller compared with the $LSCO_{113}$ region, indicating that these films are partially covered or partially coherent films, which is consistent with the growth mode

dx.doi.org/10.1021/jz500293d | J. Phys. Chem. Lett. 2014, 5, 1027−1034

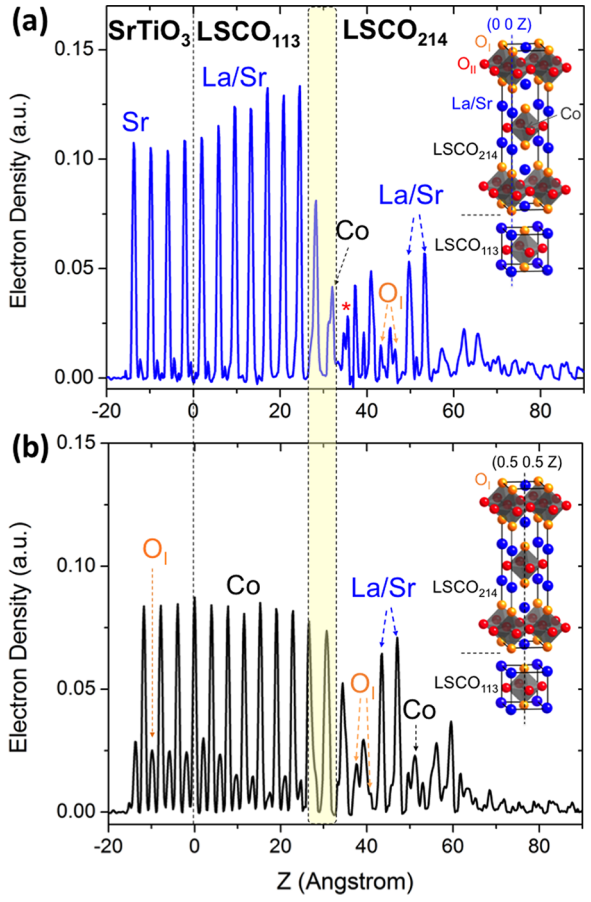

Figure 2. COBRA-determined electron density (EDY) of as-deposited $LSCO_{214}/LSCO_{113}/STO$ along: (a) the (0 0 Z) line and (b) the (0.5 0.5 Z) line. The yellow shaded region around Z = 30 Å and the dashed line at Z = 0 Å represents the $LSCO_{214}/LSCO_{113}$ and $LSCO_{113}/SrTiO_3$ interfaces, respectively.

proposed previously from the AFM images and RHEED oscillations (Figures S1 and S2, Supporting Information).

The as-deposited and annealed diffraction intensities were found to be similar (Figure 1), and the differences between the as-deposited and annealed EDYs were found to be on the order of the experimental uncertainty (Figure S3, Supporting Information). Significant changes in the surface morphology upon annealing were nevertheless observed by AFM (Figure S1, Supporting Information). We interpret this to indicate that particulates and outgrowths are present at the surface (without coherence to the substrate and therefore not detected by COBRA), and these features indeed change upon annealing, without effect on the majority of the material. It is proposed that surface Sr segregation rather than surface morphologies alone may play an important role in the surface oxygen exchange kinetics at elevated temperatures but further studies are needed to test this hypothesis.

The atomic positions in the Z direction were determined by fitting Gaussians to the EDY peaks in Figure 2. Using an ideal STO crystal frame of reference, extended throughout the entirety of the film, we plotted out the substrate relative displacement (SRD) profile for each element in $LSCO_{113}$ region (Figure S4, Supporting Information). Increasing polarization of the $LSCO_{113}$ unit cell was observed, with the octahedra displaced relative to the (La,Sr) ions. This polarization is identical in direction to distortions in $LSCO_{113}$ films observed recently;[26] however, in that work we did not observe the displacement of Co or equatorial oxygen ions. The precise physical origin is beyond the scope of this work but merits further investigation as a potential contributor to the enhanced catalytic activity of the $LSCO_{214}$-on-$LSCO_{113}$ system.

Oxygen at the $LSCO_{214}/LSCO_{113}$ interface behaved differently from oxygen within the $LSCO_{113}$ or $LSCO_{214}$ film, which can be clearly visualized from the 2D folded unit cell through a number of in-plane EDYs at different depths of the film (Figure S5, Supporting Information). In these plane-cuts, the positions of oxygen atoms is well-defined for the $Ti-O_{II}$ plane of the substrate, $Co-O_{II}$ plane of the $LSCO_{113}$ film, and $La(Sr)-O_I$ plane of the $LSCO_{214}$ film. However, near the $LSCO_{113}/LSCO_{214}$ interface, the oxygen EDY is smeared in both the $Co-O_{II}$ plane and La(Sr)-O_I planes (Figure S5, Supporting Information). This observation indicates a wider distribution of in-plane positions for oxygen atoms at the interface, which can result from the displacement of oxygen atoms from the centrosymmetric crystallographic sites or decrease in site occupancy. Similar behavior was observed previously at the interface of $LSCO_{113}$ films and surface $SrCoO_x$ particles.[26] The poor registry of oxygen atoms with the substrate-defined lattice indicates the presence of oxygen vacancies or increased oxygen mobility at the $LSCO_{214}$-on-$LSCO_{113}$ interface.

Experimental differential COBRA data and fits of the as-deposited LSCO film are in good agreement (Figure 3), from

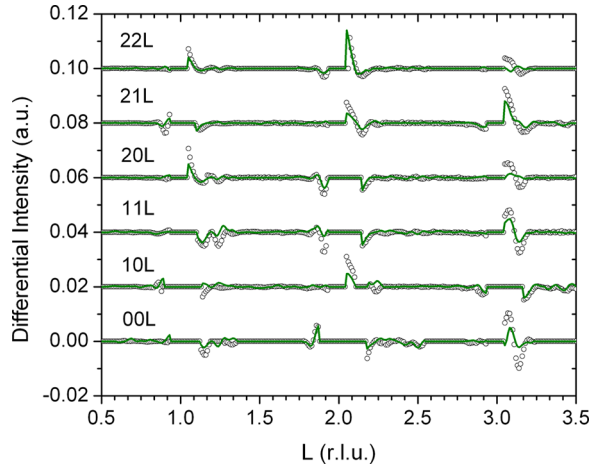

Figure 3. Differential COBRA data (black circles) and fit (green lines) for the as-deposited sample.

which the Sr concentration depth profile along the corresponding thin-film structure based from ordinary COBRA was obtained, as shown in Figure 4. The LSCO film (0—26 Å) and the topmost few layers in the STO are almost completely depleted of Sr and partially replaced by La, suggesting a $La_{1-x}CoO_3/La_{1-x}TiO_3$-like film chemistry at the $LSCO_{113}/STO$ interface. This Sr deficiency at the film/substrate interface was also found in our previous study of $LSCO_{113}/STO$, which we attributed to the oxidizing nature of the STO substrate during the film growth.[26] Such an interface can introduce a dipole moment that points toward the film/substrate interface, which may induce the aforementioned polarization of the $LSCO_{113}$ unit cell. More significantly, Sr was found to strongly segregate near the $LSCO_{214}/LSCO_{113}$ interface and in the first two to three layers of $LSCO_{214}$ from the surface, with a mean Sr occupancy of ~1 in $LSCO_{113}$ and ~1 in $LSCO_{214}$. Because the

dx.doi.org/10.1021/jz500293d | J. Phys. Chem. Lett. 2014, 5, 1027−1034

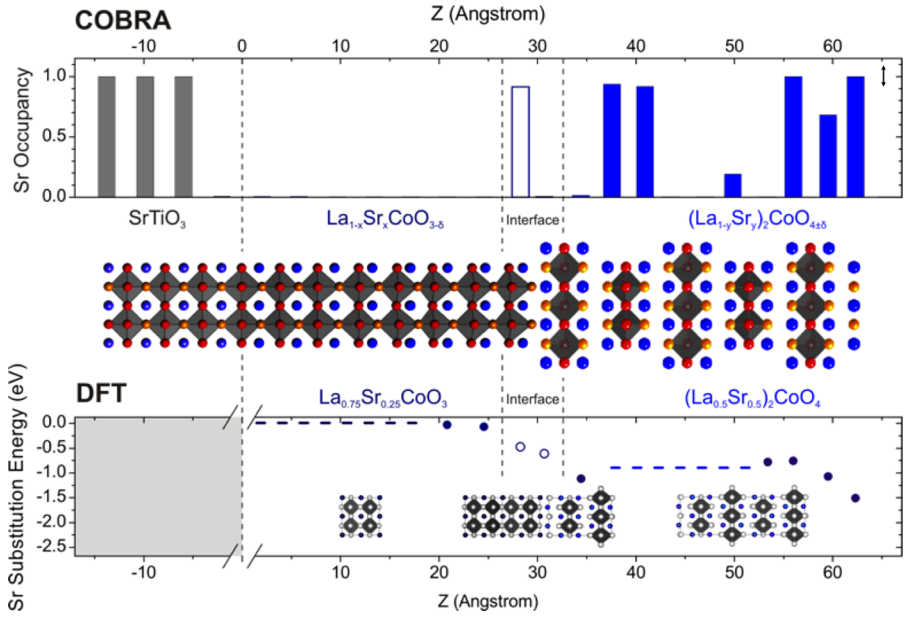

Figure 4. Top panel: Layer-by-layer Sr concentration versus depth profile determined from differential COBRA for the as-deposited LSCO thin film. The double arrow on the top-right corner indicates the uncertainty in Sr concentration. The region between two dashed black lines close to Z = 30 Å and the dashed line at Z = 0 Å represents the $(La_{1-y}Sr_y)_2CoO_{4\pm\delta}$ ($LSCO_{214}$)/$La_{1-x}Sr_xCoO_{3-\delta}$ ($LSCO_{113}$) and $LSCO_{113}$/$SrTiO_3$ (STO) interfaces, respectively. Middle panel: The schematic atomic model of the heterostructured film reflects results obtained by ordinary COBRA. Bottom panel: Ab initio Sr for La substitution energies (relative to that of bulk $La_{0.75}Sr_{0.25}CoO_3$) of bulk $La_{0.75}Sr_{0.25}CoO_3$ (dark-blue dashed line), the $(La_{0.5}Sr_{0.5})_2CoO_4$/$La_{0.75}Sr_{0.25}CoO_3$ heterointerface (filled circles between Z = 20 and 35 Å), bulk $(La_{0.5}Sr_{0.5})_2CoO_4$ (light-blue dashed line), and $(La_{0.5}Sr_{0.5})_2CoO_4$ surface (filled circles at Z > 52 Å). The horizontal dashed lines represent data from bulk supercell calculations of the relevant phases and therefore have no influence from the interfaces. The calculated La for Sr substitution energy in $SrTiO_3$ (not shown in the Figure) is found to be +2.4 eV relative to that of $La_{0.75}Sr_{0.25}CoO_3$. The schematics in the bottom Figure represent the simulated supercells for the bulk $La_{0.75}Sr_{0.25}CoO_3$, $(La_{0.5}Sr_{0.5})_2CoO_4$/$La_{0.75}Sr_{0.25}CoO_3$ heterointerface and $(La_{0.5}Sr_{0.5})_2CoO_4$ surface.

error of Sr occupancy in each layer is approximately ±10%, the average Sr occupancy of the entire film remains consistent with the nominal Sr concentration: 0.2 in $La_{1-x}Sr_xCoO_{3-\delta}$ and 0.5 in $(La_{1-y}Sr_y)_2CoO_{4\pm\delta}$. This finding provides the first experimental measurements of absolute Sr atomic occupancy of $LSCO_{214}$ on the atomic scale, which reveals for the first time clear evidence of Sr segregation on the $LSCO_{214}$ surface, and supports Sr segregation in $LSCO_{214}$ at the $LSCO_{214}$/$LSCO_{113}$ interface predicated from recent DFT studies.[19]

To further understand the physical origin of Sr segregation in the $LSCO_{214}$-on-$LSCO_{113}$ bilayer, we performed ab initio calculations to understand the thermodynamic driving force for Sr substitution of La in the structures of $LSCO_{214}$ and $LSCO_{113}$. The Sr-for-La-substitution (Sr_{La}) energies for the film away from interfaces were first approximated using those found in bulk $LSCO_{113}$ and bulk $LSCO_{214}$ (dashed lines, Figure 4), which was referenced to that in $LSCO_{113}$. The substitution energy for each atomic layer near the $LSCO_{214}$/$LSCO_{113}$ interface and in $LSCO_{214}$ was then calculated (circles, Figure 4) and compared with that in $LSCO_{113}$. Sr_{La} substitution was found to be thermodynamically more stable at the $LSCO_{113}$/$LSCO_{214}$ interface (up to approximately −0.8 eV/Sr), which was in agreement with our previous work.[19] Moreover, the thermodynamic driving force for Sr segregation near the $LSCO_{214}$ surface was even greater than that near the $LSCO_{113}$/$LSCO_{214}$ interface, with values up to approximately −1.5 eV/Sr compared with $LSCO_{113}$. This result is consistent with the strong Sr segregation in the first two to three layers from the $LSCO_{214}$ surface obtained from differential COBRA measurements. It should be mentioned that such segregation was present after PLD growth and also after subsequent annealing in air, and no significant changes was found in the Sr distribution in the film after the annealing (Figure S6, Supporting Information). This result supports the fact that the segregation is an equilibrium phenomenon, consistent with the DFT-predicted segregation tendencies.

Differential COBRA data of both as-deposited and annealed $LSCO_{214}$-on-$LSCO_{113}$ films further revealed the presence of A-site cationic ordering in the $LSCO_{214}$ film. The alternating Sr-rich and Sr-depleted layers in $LSCO_{214}$ (Figure 4 and Figure S6 in the Supporting Information) suggest that La and Sr may order in the films. Preliminary DFT results showed that there was weak thermodynamic driving force for cation ordering in $LSCO_{214}$, which can be further enhanced by strains (Figures S7 and S8 in the Supporting Information) and oxygen Frenkel pair defects (Figure S9 in the Supporting Information). Further studies are needed to allow the quantitative prediction of the chemical compositions of A-site ordering by performing full $LSCO_{214}$/$LSCO_{113}$ heterointerface modeling, as we have sampled only a small fraction of possible chemical configurations in this work. (Details are provided in the Supporting Information.)

The Sr segregation at the $LSCO_{214}$-on-$LSCO_{113}$ revealed by the COBRA measurements provides fundamental insights that can explain the enhanced surface oxygen exchange kinetics previously reported.[15] Sr segregation (Sr occupancy on the A site of ∼1) in the perovskite structure at the $LSCO_{214}$/$LSCO_{113}$ interface can lift the oxygen 2p band center relative to the Fermi level,[35,36] shown by DFT studies, which is correlated with increasing surface oxygen kinetics.[35] In addition, such Sr segregation can promote oxygen ion transport kinetics as higher Sr concentrations in bulk $LSCO_{113}$[37] increase the oxygen

dx.doi.org/10.1021/jz500293d | J. Phys. Chem. Lett. 2014, 5, 1027−1034

vacancy concentration due to the charge imbalance from the substitution of Sr^{2+} for La^{3+} in the perovskite structure,[19,20] which is supported by the weak EDY of oxygen ions in the $LSCO_{214}/LSCO_{113}$ interface in Figure 2 (indicative of a local increase in the oxygen vacancy concentration and oxygen ion mobility). Because $LSCO_{214}$ only partially covers $LSCO_{113}$, the Sr occupancy equal to ~1 in the $LSCO_{214}/LSCO_{113}$ interface indicates the surface layer of the $LSCO_{113}$ base film contains fully occupied Sr at the A-sites while the previously reported $LSCO_{113}$ base film (without $LSCO_{214}$) has a surface layer at lower Sr occupancy (~0.6).[26] Considering the correlation between the computed O 2p band center (relative to the Fermi level) and the oxygen surface exchange kinetics for perovskites,[35] here we show that the O 2p band center versus the Fermi level of $LSCO_{113}$ interface layer is lifted upward with increasing Sr occupancy (Figure 5). In addition, although the dominant oxygen defects in $LSCO_{214}$ can be oxygen vacancies or oxygen interstitials (which dominates is dependent on the Sr concentration,[38] oxygen partial pressure, and temperature), it is proposed that oxygen vacancies are the dominant anionic defect for Sr-segregated $LSCO_{214}$-on-$LSCO_{113}$ surface under SOFC conditions based on previous findings of $LSCO_{214}$ defect concentrations. Specifically, $LSCO_{214}$ has been found to have understoichiometry ~0.1 for Sr occupancies greater than 1.5 in air at 704 °C.[39] Figure 5 shows the surface-exchange activity as a function of the bulk O 2p band center for the $LSCO_{214}$ and select other materials, and it is seen that the fully Sr-occupied top surface layer of the $LSCO_{214}$ islands on the $LSCO_{113}$ film also contains a higher O 2p band center than the surface layer of the particles on the $LSCO_{113}$ film, which could lead to higher activities. At the Sr occupancy of ~1 near both the $LSCO_{214}/LSCO_{113}$ interface and the $LSCO_{214}$ surface, as detected by differential COBRA, the position of the computed O 2p band center relative to the Fermi level becomes comparable to the most active perovskites (i.e., $Ba_{1-x}Sr_xCo_{1-y}Fe_yO_{3-\delta}$, BSCF) for surface oxygen exchange kinetics.[35] Therefore, the unique Sr occupancy changes within the $LSCO_{214}$-on-$LSCO_{113}$ heterostructure might be responsible for the enhanced surface-exchange kinetics relative to $LSCO_{113}$. It should be noted that our observation of Sr segregation in the perovskite lattice is distinct from the precipitation of nonperovskite Sr-rich secondary phases (most likely not coherent with the perovskite structure), which might also be present but are not detectable by COBRA. These secondary particles, if sufficiently thick, can block surface reaction sites and impede ORR kinetics.[21,22] Caution should also be given to the proposed correlation between the atomic structure information of films grown STO obtained from COBRA and surface-exchange kinetics obtained from films grown on YSZ, as the atomic positions and Sr segregation in $LSCO_{113}$ and $LSCO_{214}$ may vary depending on film-deposition conditions and substrate.[26] Nevertheless, understanding the driving forces that yield this nonuniform Sr distribution and potentially controlling surface Sr segregation represents a critical next step in designing oxides with high activities and stability for surface-exchange kinetics.

In summary, we have investigated the $LSCO_{214}$-on-$LSCO_{113}$ heterostructure using COBRA and ab initio calculations to provide, for the first time, atomic-scale structural and chemical information. Different COBRA analysis reveals significant Sr segregation at the interface of $LSCO_{214}/LSCO_{113}$ (within the rocksalt layer shared between $LSCO_{214}$ and $LSCO_{113}$) and near the surface of $LSCO_{214}$. Ab initio calculations show that such pronounced Sr segregation can be attributed to a reduction in

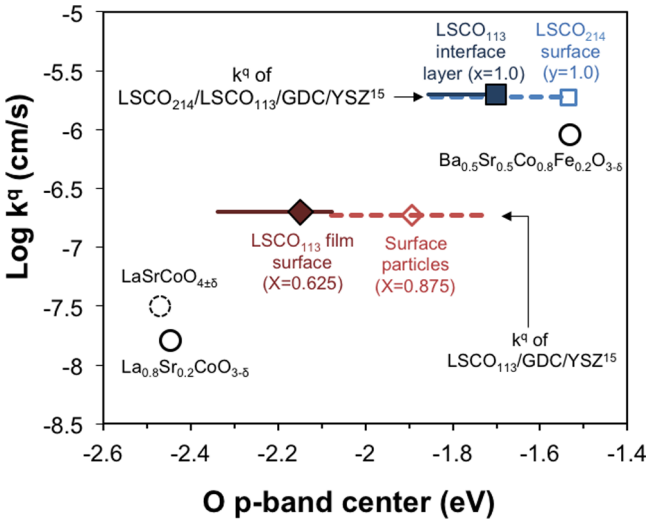

Figure 5. Surface exchange coefficients k^q or k^* versus the calculated O 2p band centers (relative to the Fermi level) calculated for bulk unit cells. The specific details for each data point are as follows. k^q values are shown for uncoated $La_{0.8}Sr_{0.2}CoO_{3-\delta}$ films ($LSCO_{113}$, red diamonds) and $(La_{0.5}Sr_{0.5})_2CoO_{4\pm\delta}$ ($LSCO_{214}$, blue squares) covered $LSCO_{113}$ films, both on the yttria-stabilized zirconia (001) single crystals buffered by a gadolinium-doped ceria layer at T = 550 °C, $P(O_2)$= 1 bar.[15] Each of these cases has associated with two separate O 2p band center values corresponding to two possible compositions used in the bulk calculations for each case, which compositions are estimated from COBRA measurements of the most relevant active surface or interface layers. Although the compositions are estimated from surface or interface compositions, the O 2p band center calculations are done with bulk unit cells. For uncoated $LSCO_{113}$ film,[26] we use a bulk composition of $La_{1-x}Sr_xCoO_3$ at x = 0.625 (red filled diamond), as previous COBRA measurements reveal Sr segregation on the $LSCO_{113}$ film surface to x = 0.59.[26] For the $LSCO_{214}$-on-$LSCO_{113}$ film, we use a bulk composition of $La_{1-x}Sr_xCoO_3$ at x = 1 (blue filled squares), as the interface layer of the $LSCO_{214}$-on-$LSCO_{113}$ heterostructure is near x = 1, as revealed in Figure 4. The possible error in the COBRA measurement for the Sr occupancy (~10%) is represented by the thin horizontal bars. Bulk DFT calculations have been done to estimate the O 2p band centers at the end points of these bars, which represent compositions of x = 0.5 (left) and x = 0.75 (right) for the uncoated LSC_{113} film and x = 0.875 (left) and x = 1.0 (right) for the $LSCO_{214}$-on-$LSCO_{113}$ film. A similar assessment for k^q values of the uncoated $LSCO_{113}$ and LSCO214-on-$LSCO_{113}$ film versus the calculated O 2p band centers (relative to the Fermi level) of bulk $La_{1-x}S_xCoO_3$ and $(La_{1-y}Sr_y)_2CoO_4$ based on the compositions of the top surface of Sr-segregated particles on the $LSCO_{113}$ film[26] (x = 0.875, open red triangle) and the top surface layer of $LSCO_{214}$ islands on the $LSCO_{113}$ of $LSCO_{214}$-on-$LSCO_{113}$ (y = 1.0, open blue square), respectively, was carried out. Again, the possible error in the COBRA measurement for the Sr occupancy (10%) represented by the horizontal dashed bars. The end points of the bars represent compositions of x = 0.75 (left) and x = 1.0 (right) for the uncoated LSC_{113} film and x = 0.875 (left) and x = 1.0 (right) for the $LSCO_{214}$-on-$LSCO_{113}$ film. The black circles are the reported experimental k^* of bulk $LSCO_{113}$[47] and $Ba_{0.5}Sr_{0.5}Co_{0.8}Fe_{0.2}O_{3-\delta}$ (BSCF)[48] at $p(O_2)$ = 1.0 bar at T = 600 °C versus the calculated bulk O 2p band centers.[35] The dashed circle is the estimated k^*_{eq} of bulk $LSCO_{214}$ at y = 0.5 at T = 600 °C and $p(O_2)$ = 1.0 bar.[19] (based on the reported interfacial conductivity of the porous $LSCO_{214}$ electrode[49]) versus the calculated bulk $(La_{0.5}Sr_{0.5})_2CoO_4$ O 2p band center. The structures used for calculating the O 2p band centers of $LSCO_{113}$ and $LSCO_{214}$ are provided in Figure S10 in the Supporting Information.

dx.doi.org/10.1021/jz500293d | J. Phys. Chem. Lett. 2014, 5, 1027−1034

the Sr_{La} substitution energy at the $LSCO_{113}/LSCO_{214}$ interface and at the surface of $LSCO_{214}$, which qualitatively agrees with the experimental Sr occupancy profile. The increased Sr content at the $LSCO_{214}/LSCO_{113}$ interface is coupled to a smearing of the oxygen EDY, indicative of higher local oxygen vacancy concentration or enhanced oxygen mobility. Our findings provide fundamental insights into unique structural and chemical information of oxide surface and interfaces that may be responsible for the enhanced catalytic activities of such oxide heterostructures for oxygen electrocatalysis at elevated temperatures.

EXPERIMENTAL AND THEORETICAL METHODS

Atomic Force Microscopy Characterization. An Asylum Research MFP-3D AFM was used to examine the surface morphology of the LSCO heterostructured film under as-deposited and annealed conditions.

Coherent Bragg Rod Analysis (COBRA). The atomic structure and Sr depth profile of the $LSCO_{214}$-on-$LSCO_{113}$ film under as-deposited and annealed conditions were investigated at beamline ID-33 of the Advanced Photon Source (APS) at Argonne National Laboratory (ANL). Procedures for measuring the diffraction intensities along the substrate-defined Bragg rods have been previously described.[26,28,29] Ordinary COBRA measurements were performed using an incident X-ray photon energy of 16.09 keV (just below the Sr absorption edge), while energy differential COBRA was performed by modulating between 16.09 and 16.11 keV (just above the Sr absorption edge). COBRA uses the measured diffraction intensities and the fact that the complex structure factors (CSFs) vary continuously along the substrate-defined Bragg rods to determine the diffraction phases of the CSFs. The CSFs are then Fourier-transformed into real space to obtain the 3D EDY of the film and substrate with sub-angstrom resolution. Energy differential COBRA provides elemental sensitivity through the energy dependence of the Sr atomic scattering factors above and below the absorption edge. Using the structural information directly obtained from ordinary COBRA, then varying the Sr concentration (i.e., occupancy of Sr) in each La/Sr layer to fit the differential intensity from the energy-modulated measurements, a depth profile of the Sr distribution can be determined.

Ab Initio Calculations. Spin-polarized DFT calculations were performed with the Vienna Ab Initio Simulation Package[40,41] using the projector-augmented plane-wave method[42] with a cutoff energy of 450 eV. Exchange-correlation was treated in the Perdew–Wang-91[43] generalized gradient approximation (GGA) using the soft O_s oxygen pseudopotential (which includes $2s^2$ $2p^4$ electronic configuration). The GGA+U calculations[44] were performed with the simplified spherically averaged approach,[45] where the U_{eff} (U_{eff} = coulomb U-exchange J) is applied to Co d electrons (U_{eff} = 3.3 eV). All calculations were performed in the ground-state ferromagnetic arrangement to use a consistent and tractable set of magnetic structures. While elevated temperatures used during synthesis and electrochemical testing in this study are expected to be in a paramagnetic state, such disordered moments are significantly more difficult to model, and we believe that the trends and conclusions identified here would not be altered by using random spin arrangements. Multiple previous studies on LSC and related materials, for example, $LaMnO_3$, have obtained good agreement with experimental data at high temperatures using ferromagnetic arrangements.[1,35,46]

Sr substitution (i.e., Sr replaces La) energy calculations of bulk $LSCO_{113}$, $LSCO_{214}$, $LSCO_{113}$–$LSCO_{214}$ heterointerfaces, and $LSCO_{214}$ surfaces were performed as follows. The $LSCO_{113}$–$LSCO_{214}$ heterointerface was simulated with a fully periodic 176-atom supercell ($2a_{113} \times 2a_{113}$ supercell in the x–y plane (a_{113} = 3.85 Å) with 12 layers of $LSCO_{113}$ and 6 layers of $LSCO_{214}$ along z where c_{113} = 3.83 Å). The in-plane lattice parameter for the interface calculation was fixed to that of $LSCO_{113}$ (a_{113}). Calculations of $LSCO_{214}$ (001) free surfaces were performed using a symmetric slab with 72 atoms (the primitive $LSCO_{214}$ cell has 14 atoms) with $2a_{214} \times 2a_{214}$ in the x–y direction and both surfaces terminating with rocksalt AO–AO layers in the z direction. Bottom AO–AO layers were fixed to the bulk, and all other layers were internally relaxed. The bulk $LSCO_{214}$ structure was simulated with $2a_{214} \times 2a_{214} \times 2c_{214}$ supercell, and the bulk $LSCO_{113}$ was simulated with a four-layer or $2a_{113} \times 2a_{113} \times 2a_{113}$ supercell. The $LSCO_{113}$–$LSCO_{214}$ heterointerface structural model was reported previously,[19] and the simulated bulk $LSCO_{113}$, $LSCO_{214}$, and $LSCO_{214}$ surface slab model is provided in Figure 4. Dipole correction in the direction orthogonal to the free surface was included in all surface slab simulations to correct for the dipole effect due to the asymmetry caused by Sr-substitution at/near the surface. Sr substitution energy was calculated by taking the total energy change from the stoichiometric supercell after one La ion is replaced by Sr. More details of the calculation methods in this study can be found in the Supporting Information.

ASSOCIATED CONTENT

Supporting Information

Details of sample preparation, ordinary and differential COBRA analysis, error analysis, and octahedral distortion and ab initio calculations. This material is available free of charge via the Internet at http://pubs.acs.org.

AUTHOR INFORMATION

Corresponding Authors

*E-mail: ddmorgan@wis.edu.

*E-mail: shaohorn@mit.edu.

Notes

The authors declare no competing financial interest.

ACKNOWLEDGMENTS

This work was partially supported by DOE (SISGR DESC0002633) and King Abdullah University of Science and Technology. We thank the King Fahd University of Petroleum and Minerals in Dharam, Saudi Arabia for funding the research reported in this paper through the Center for Clean Water and Clean Energy at MIT and KFUPM. This research was supported by the Israel Science Foundation under grant no. 1005/11. Support for Y.-L.L. was provided by Department of Energy (DOE), National Energy Technology Laboratory (NETL), Solid State Energy Conversion Alliance (SECA) Core Technology Program, Funding Opportunity Number DEFE0009435, and that for M.J.G. was provided by U.S. Department of Energy, Office of Basic Energy Sciences, Division of Materials Sciences and Engineering under award number DESC0001284. Use of the Advanced Photon Source, an Office of Science User Facility operated for the U.S. Department of Energy (DOE) Office of Science by Argonne National Laboratory was supported by the U.S. DOE under

Contract No. DE-AC02-06CH11357. We acknowledge the support from the beamline scientists including Zhan Zhang, Christian M. Schlepuetz, and Lynette Jirik at ID-33 of APS. Samples were synthesized at the Center for Nanophase Materials Sciences, which is sponsored at Oak Ridge National Laboratory by the Scientific User Facilities Division, Office of Basic Energy Sciences, U.S. DOE under Contract No. CNMS2012-284.

REFERENCES

(1) Lee, Y. L.; Kleis, J.; Rossmeisl, J.; Morgan, D. Ab Initio Energetics of $LaBO_3$(001) (B = Mn, Fe, Co, and Ni) for Solid Oxide Fuel Cell Cathodes. *Phys. Rev. B* **2009**, *80*, 224101.

(2) Adler, S. B. Factors Governing Oxygen Reduction in Solid Oxide Fuel Cell Cathodes. *Chem. Rev.* **2004**, *104*, 4791−4843.

(3) Suntivich, J.; Gasteiger, H. A.; Yabuuchi, N.; Nakanishi, H.; Goodenough, J. B.; Shao-Horn, Y. Design Principles for Oxygen-Reduction Activity on Perovskite Oxide Catalysts for Fuel Cells and Metal-Air Batteries. *Nat. Chem.* **2011**, *3*, 647−647.

(4) Suntivich, J.; May, K. J.; Gasteiger, H. A.; Goodenough, J. B.; Shao-Horn, Y. A Perovskite Oxide Optimized for Oxygen Evolution Catalysis from Molecular Orbital Principles. *Science* **2011**, *334*, 1383−1385.

(5) Kim, C. H.; Qi, G. S.; Dahlberg, K.; Li, W. Strontium-Doped Perovskites Rival Platinum Catalysts for Treating NOx in Simulated Diesel Exhaust. *Science* **2010**, *327*, 1624−1627.

(6) Gorte, R. J.; Vohs, J. M. Catalysis in Solid Oxide Fuel Cells. *Annu. Rev. Chem. Biomol.* **2011**, *2*, 9−30.

(7) Orikasa, Y.; Ina, T.; Nakao, T.; Mineshige, A.; Amezawa, K.; Oishi, M.; Arai, H.; Ogumi, Z.; Uchimoto, Y. X-ray Absorption Spectroscopic Study on $La_{0.6}Sr_{0.4}CoO_{3-\delta}$ Cathode Materials Related with Oxygen Vacancy Formation. *J. Phys. Chem. C* **2011**, *115*, 16433−16438.

(8) Dusastre, V.; Kilner, J. A. Optimisation of Composite Cathodes for Intermediate Temperature SOFC Applications. *Solid State Ionics* **1999**, *126*, 163−174.

(9) Chen, Y.; Cai, Z. H.; Kuru, Y.; Ma, W.; Tuller, H. L.; Yildiz, B. Electronic Activation of Cathode Superlattices at Elevated Temperatures − Source of Markedly Accelerated Oxygen Reduction Kinetics. *Adv. Energy Mater.* **2013**, *3*, 1221−1229.

(10) Goodenough, J. B. Electronic and Ionic Transport Properties and Other Physical Aspects of Perovskites. *Rep. Prog. Phys.* **2004**, *67*, 1915−1993.

(11) Kendall, K. R.; Navas, C.; Thomas, J. K.; zurLoye, H. C. Recent Developments in Perovskite-Based Oxide Ion Conductors. *Solid State Ionics* **1995**, *82*, 215−223.

(12) Carter, S.; Selcuk, A.; Chater, R. J.; Kajda, J.; Kilner, J. A.; Steele, B. C. H. Oxygen-Transport in Selected Nonstoichiometric Perovskite-Structure Oxides. *Solid State Ionics* **1992**, *53*, 597−605.

(13) Sase, M.; Hermes, F.; Yashiro, K.; Otake, T.; Kaimai, A.; Kawada, T.; Mizusaki, J.; Sakai, N.; Yamaji, K.; Horita, T.; Yokokawa, H. Fast 18O Incorporation Paths along the Hetero Phase Boundary with $(La,Sr)CoO_3/(La,Sr)_2CoO_4$. 7th European SOFC Forum, Luzern; Bossel, U., Ed.; Luzern, 2006; p B-66.

(14) Sase, M.; Hermes, F.; Yashiro, K.; Sato, K.; Mizusaki, J.; Kawada, T.; Sakai, N.; Yokokawa, H. Enhancement of Oxygen Surface Exchange at the Hetero-Interface of $(La,Sr)CoO_3/(La,Sr)_2CoO_4$ with PLD-Layered Films. *J. Electrochem. Soc.* **2008**, *155*, B793−B797.

(15) Crumlin, E. J.; Mutoro, E.; Ahn, S. J.; la O', G. J.; Leonard, D. N.; Borisevich, A.; Biegalski, M. D.; Christen, H. M.; Shao-Horn, Y. Oxygen Reduction Kinetics Enhancement on a Heterostructured Oxide Surface for Solid Oxide Fuel Cells. *J. Phys. Chem. Lett.* **2010**, *1*, 3149−3155.

(16) Sase, M.; Yashiro, K.; Sato, K.; Mizusaki, J.; Kawada, T.; Sakai, N.; Yamaji, K.; Horita, T.; Yokokawa, H. Enhancement of Oxygen Exchange at the Hetero Interface of $(La,Sr)CoO_3/(La,Sr)_2CoO_4$ in Composite Ceramics. *Solid State Ionics* **2008**, *178*, 1843−1852.

(17) la O', G. J.; Ahn, S. J.; Crumlin, E.; Orikasa, Y.; Biegalski, M. D.; Christen, H. M.; Shao-Horn, Y. Catalytic Activity Enhancement for Oxygen Reduction on Epitaxial Perovskite Thin Films for Solid-Oxide Fuel Cells. *Angew. Chem., Int. Ed.* **2010**, *49*, 5344−5347.

(18) Mutoro, E.; Crumlin, E. J.; Biegalski, M. D.; Christen, H. M.; Shao-Horn, Y. Enhanced Oxygen Reduction Activity on Surface-Decorated Perovskite Thin Films for Solid Oxide Fuel Cells. *Energy Environ. Sci.* **2011**, *4*, 3689−3696.

(19) Gadre, M. J.; Lee, Y. L.; Morgan, D. Cation Interdiffusion Model for Enhanced Oxygen Kinetics at Oxide Heterostructure Interfaces. *Phys. Chem. Chem. Phys.* **2012**, *14*, 2606−2616.

(20) Crumlin, E. J.; Mutoro, E.; Liu, Z.; Grass, M. E.; Biegalski, M. D.; Lee, Y. L.; Morgan, D.; Christen, H. M.; Bluhm, H.; Shao-Horn, Y. Surface Strontium Enrichment on Highly Active Perovskites for Oxygen Electrocatalysis in Solid Oxide Fuel Cells. *Energy Environ. Sci.* **2012**, *5*, 6081−6088.

(21) Ding, H. P.; Virkar, A. V.; Liu, M. L.; Liu, F. Suppression of Sr Surface Segregation in $La_{1-x}Sr_xCo_{1-y}Fe_yO_{3-\delta}$: a First Principles Study. *Phys. Chem. Chem. Phys.* **2013**, *15*, 489−496.

(22) Chen, Y.; Jung, W.; Cai, Z. H.; Kim, J. J.; Tuller, H. L.; Yildiz, B. Impact of Sr Segregation on the Electronic Structure and Oxygen Reduction Activity of $SrTi_{1-x}Fe_xO_3$ Surfaces. *Energy Environ. Sci.* **2012**, *5*, 7979−7988.

(23) Cai, Z. H.; Kubicek, M.; Fleig, J.; Yildiz, B. Chemical Heterogeneities on $La_{0.6}Sr_{0.4}CoO_{3-\delta}$ Thin Films-Correlations to Cathode Surface Activity and Stability. *Chem. Mater.* **2012**, *24*, 1116−1127.

(24) Feng, Z.; Crumlin, E. J.; Hong, W. T.; Lee, D.; Mutoro, E.; Biegalski, M. D.; Zhou, H.; Bluhm, H.; Christen, H. M.; Shao-Horn, Y. In Situ Studies of Temperature-Dependent Surface Structure and Chemistry of Single-Crystalline (001) Oriented $La_{0.8}Sr_{0.2}CoO_{3-\delta}$ Perovskite Thin Films. *J Phys. Chem. Lett.* **2013**, *4*, 1512−1518.

(25) Kubicek, M.; Limbeck, A.; Fromling, T.; Hutter, H.; Fleig, J. Surface Cation Segregation and its Effect on the Oxygen Reduction Reaction on Mixed Conducting Electrodes Investigated by ToF-SIMS and ICP-OES. *ECS Trans.* **2011**, *35*, 1975−1983.

(26) Feng, Z.; Yacoby, Y.; Hong, W. T.; Zhou, H.; Biegalski, M. D.; Christen, H. M.; Shao-Horn, Y. Revealing the Atomic Structure and Strontium Distribution in Nanometer-Thick $La_{0.8}Sr_{0.2}CoO_{3-\delta}$ Grown on (001)-Orientated $SrTiO_3$. *Energy Environ. Sci.* **2014**, *7*, 1166−1174.

(27) Yacoby, Y.; Sowwan, M.; Stern, E.; Cross, J. O.; Brewe, D.; Pindak, R.; Pitney, J.; Dufresne, E. M.; Clarke, R. Direct Determination of Epitaxial Interface Structure in Gd_2O_3 Passivation of GaAs. *Nat. Mater.* **2002**, *1*, 99−101.

(28) Sowwan, M.; Yacoby, Y.; Pitney, J.; MacHarrie, R.; Hong, M.; Cross, J.; Walko, D. A.; Clarke, R.; Pindak, R.; Stern, E. A. Direct Atomic Structure Determination of Epitaxially Grown Films: Gd_2O_3 on GaAs(100). *Phys. Rev. B* **2002**, *66*, 205311.

(29) Yacoby, Y.; Brooks, C.; Schlom, D.; Cross, J. O.; Walko, D. A.; Cionca, C. N.; Husseini, N. S.; Riposan, A.; Clarke, R. Structural Changes Induced by Metal Electrode Layers on Ultrathin $BaTiO_3$ films. *Phys. Rev. B* **2008**, *77*, 195426.

(30) Yacoby, Y.; Zhou, H.; Pindak, R.; Bozovic, I. Atomic-Layer Synthesis and Imaging Uncover Broken Inversion Symmetry in $La_{2-x}Sr_xCuO_4$ Films. *Phys. Rev. B* **2013**, *87*, 014108.

(31) Yacoby, Y.; Elfassy, N.; Ray, S. K.; Singha, R. K.; Das, S.; Cohen, E.; Yochelis, S.; Clarke, R.; Paltiel, Y. Morphology and Growth of Capped Ge/Si Quantum Dots. *J. Nanopart. Res.* **2013**, *15*, 1608.

(32) Kubicek, M.; Limbeck, A.; Fromling, T.; Hutter, H.; Fleig, J. Relationship between Cation Segregation and the Electrochemical Oxygen Reduction Kinetics of $La_{0.6}Sr_{0.4}Co\ O_{3-\delta}$ Thin Film Electrodes. *J. Electrochem. Soc.* **2011**, *158*, B727−B734.

(33) Zhou, H.; Yacoby, Y.; Butko, V. Y.; Logvenov, G.; Bozovic, I.; Pindak, R. Anomalous Expansion of the Copper-Apical-Oxygen Distance in Superconducting Cuprate Bilayers. *Proc. Natl. Acad. Sci. U.S.A.* **2010**, *107*, 8103−8107.

(34) Zhou, H.; Pindak, R.; Clarke, R.; Steinberg, D. M.; Yacoby, Y. The Limits of Ultrahigh-Resolution X-ray Mapping: Estimating

Uncertainties in Thin-Film and Interface Structures Determined by Phase Retrieval Methods. *J. Phys. D: Appl. Phys.* **2012**, *45*, 195302.
(35) Lee, Y. L.; Kleis, J.; Rossmeisl, J.; Shao-Horn, Y.; Morgan, D. Prediction of Solid Oxide Fuel Cell Cathode Activity with First-Principles Descriptors. *Energy Environ. Sci.* **2011**, *4*, 3966−3970.
(36) Grimaud, A.; May, K. J.; Carlton, C. E.; Lee, Y. L.; Risch, M.; Hong, W. T.; Zhou, J.; Shao-Horn, Y. Double Perovskite as a Family of Highly Active Catalysts For Oxygen Evolution in Alkaline Solution. *Nat. Commun.* **2013**, *4*, 2439.
(37) Mizusaki, J.; Mima, Y.; Yamauchi, S.; Fueki, K.; Tagawa, H. Nonstoichiometry of the Perovskite-Type Oxides $La_{1-x}Sr_xCoO_{3-\delta}$. *J. Solid State Chem.* **1989**, *80*, 102−111.
(38) Tealdi, C.; Ferrara, C.; Mustarelli, P.; Islam, M. S. Vacancy and Interstitial Oxide Ion Migration in Heavily Doped $La_{2-X}Sr_xCoO_{4\pm\delta}$. *J. Mater. Chem.* **2012**, *22*, 8969−8975.
(39) Prasanna, T. R. S.; Navrotsky, A. Energetics of $La_{2-X}Sr_xCoO_{4-y}$ ($0.5 < x < 1.5$). *J. Solid State Chem.* **1994**, *112*, 192−195.
(40) Kresse, G.; Hafner, J. Ab Initio Molecular Dynamics for Liquid Metals. *Phys. Rev. B* **1993**, *47*, 558.
(41) Kresse, G.; Furthmuller, J. Efficient Iterative Schemes for Ab Initio Total-Energy Calculations Using a Plane-Wave Basis Set. *Phys. Rev. B* **1996**, *54*, 11169−11186.
(42) Blochl, P. E. Projector Augmented-Wave Method. *Phys. Rev. B* **1994**, *50*, 17953−17979.
(43) Perdew, J. P.; Wang, Y. Accurate and Simple Analytic Representation of the Electron-Gas Correlation Energy. *Phys. Rev. B* **1992**, *45*, 13244.
(44) Anisimov, V. I.; Aryasetiawan, F.; Lichtenstein, A. I. First-Principles Calculations of the Electronic Structure and Spectra of Strongly Correlated Systems: The LDA+U Method. *J. Phys.: Condens. Matter* **1997**, *9*, 767−808.
(45) Dudarev, S. L.; Botton, G. A.; Savrasov, S. Y.; Humphreys, C. J.; Sutton, A. P. Electron- Energy-Loss Spectra and the Structural Stability of Nickel Oxide: An LSDA+U Study. *Phys. Rev. B* **1998**, *57*, 1505−1509.
(46) Lee, Y. L.; Morgan, D. Ab Initio and Empirical Defect Modeling of $LaMnO_{3\pm\delta}$ for Solid Oxide Fuel Cell Cathodes. *Phys. Chem. Chem. Phys.* **2012**, *14*, 290−302.
(47) De Souza, R. A.; Kilner, J. A. Oxygen Transport in $La_{1-x}Sr_xMn_{1-y}Co_yO_{3\pm\delta}$ Perovskites Part II. Oxygen Surface Exchange. *Solid State Ionics* **1999**, *126*, 153−161.
(48) Wang, L.; Merkle, R.; Maier, J. Surface Kinetics and Mechanism of Oxygen Incorporation Into $Ba_{1-x}Sr_xCo_yFe_{1-y}O_{3-\delta}$ SOFC Micro-electrodes. *J. Electrochem. Soc.* **2010**, *157*, B1802−B1808.
(49) Yashiro, K.; Nakamura, T.; Sase, M.; Hermes, F.; Sato, K.; Kawada, T.; Mizusaki, J. Composite Cathode of Perovskite-Related Oxides, $(La,Sr)CoO_{3-\delta}/(La,Sr)_2CoO_{4-\delta}$, for Solid Oxide Fuel Cells. *Electrochem. Solid St.* **2009**, *12*, B135−B137.